Nuclear Instruments and Methods in Physics Research B 535 (2023) 137–148

Contents lists available at ScienceDirect

Nuclear Inst. and Methods in Physics Research, B

journal homepage: www.elsevier.com/locate/nimb

Improved methods for calculating electron, positron, and photon radiation-induced displacement damage cross sections

Shengli Chen [a,b,*], Dingbang Cai [a,b], David Bernard [b], Yannick Peneliau [c]

[a] Sino-French Institute of Nuclear Engineering and Technology, Sun Yat-sen University, Zhuhai 519082, Guangdong, China
[b] CEA, DES, IRESNE, DER, SPRC, LEPh, Cadarache 13108, Saint Paul Lez Durance, France
[c] CEA, IRFM, Cadarache 13108 Saint Paul Lez Durance, France

ARTICLE INFO

Keywords:
Displacement damage
Electron, positron, photon
DPA cross section
Mott cross section
Pair production

ABSTRACT

Radiation damage is a key challenge for materials. Accurate evaluation of radiation damage is a starting point for investigating the behaviors of materials used in a radiation environment. The present work proposes improved methods for calculating the primary radiation damage cross sections induced by light particles, including electrons, positrons, and photons. The main improvements compared with previous methods are: (1) accurate Mott cross section rather than the McKinley-Feshbach analytical approach is used for electron and positron scattering; (2) data and methods recommended by the International Commission on Radiation Unit and measurements (ICRU) are systematically applied for computing the stopping powers of electron and positron; (3) accurate differential cross section by combining different models instead of some simple approaches is used for pair production. The electron, positron, and photon irradiation-induced displacement cross sections for various important elements covering a large range of atomic numbers (from Li to U) are computed with the improved methods for energy up to 100 MeV. The calculated displacement cross sections are also tabulated so that they can be simply used for further applications.

1. Introduction

In a radiation environment, atoms in materials can be knocked out by kinetic particles, such as neutrons and photons. Once an atom is knocked-on, a vacancy and an interstitial atom (also known as a Frenkel pair) are formed in the material. These point defects and their evolution will largely change the properties of materials. It is thus of great importance to study the atomic displacement damage for materials used in a radiation environment. The atomic displacement damage, also called primary radiation damage [1], is conventionally quantified by the number of Displacements per Atom (DPA) of irradiated materials.

Photon (widely recognized as gamma-ray in the energy range of producing displacement damage) is an important radiation source in nuclear reactors, nuclear experimental facilities, nuclear medicine, and astrospace. The irradiation damage induced by photons needs thus to be accurately evaluated. Because the irradiation damage depends on both the radiation environment (e.g., photon spectrum and absolute flux) and the material itself, it is important to establish some pre-calculated databases that can be directly used to evaluate the irradiation damage of a specific material in any environment. Inspired by reaction cross section, the so-called damage cross section or DPA cross section is proposed. The irradiation damage rate is assessed by the inner product of the damage cross section and the flux spectrum in a specific radiation environment.

The neutron-induced damage cross sections can be now computed by the nuclear data processing code NJOY [2] or some codes having similar functionality [3–5] (even though some improvements are required [6,7]). However, there is no such tool for calculating photon irradiation damage cross sections. Simakov and Fischer showed that the contribution of the photo-nuclear effect is negligible when compared with the damage induced by photo-atomic interactions [8]. Photon irradiation induces the primary damage mainly via the three atomic level interactions: Photoelectric Effect (PE), Compton Scattering (CS), and Pair Production (PP). The methods for calculating photon irradiation-induced displacement damage cross section were firstly proposed by Oen and Holmes in 1959 [9]. Later, many works have been performed to compute the photon-induced DPA cross sections [10–14].

However, as shown in Refs. [14,15], large discrepancies are observed among different photon-induced damage cross sections. We have thoroughly analyzed previous methods, pointed out the potential issues, and recommended the methods for photon irradiation DPA cross section

* Corresponding author at: Sino-French Institute of Nuclear Engineering and Technology, Sun Yat-sen University, Zhuhai 519082, Guangdong, China.
E-mail address: chenshli23@mail.sysu.edu.cn (S. Chen).

https://doi.org/10.1016/j.nimb.2022.12.007
Received 30 May 2022; Received in revised form 6 December 2022; Accepted 7 December 2022
Available online 17 December 2022

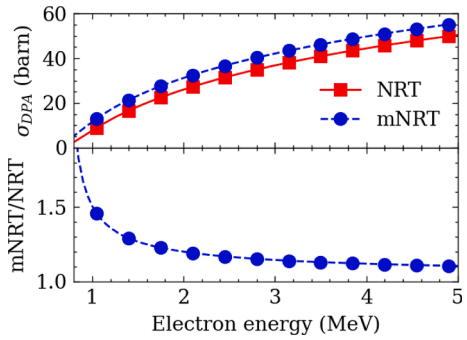

Fig. 1. Comparison of electron-induced DPA cross sections of Fe using the NRT and mNRT formulae [21].

calculation [15]. However, it should be noted that the McKinley-Feshbach approach for electron and positron (products of photo-atomic interactions) scattering is not valid for atoms with atomic number Z > 27 [16]. In addition, the form function of the PP reaction given by Fukuya and Kimura [13] has not been physically or mathematically justified. Therefore, more accurate evaluation methods need to be proposed and studied for photon irradiation displacement damage cross section calculation, especially for atoms with Z > 27.

The present work develops accurate evaluation methods for electron, positron, and photon irradiation-induced displacement damage cross sections based on fundamental interaction mechanisms. The proposed methods are detailed in Section 2. Some numerical results and the discussion are given in Section 3. The main conclusions are summarized in Section 4.

2. Methods

2.1. Electron and positron irradiation-induced displacement cross sections

As explained previously, the photo-atomic interactions induce radiation damage through the collision of electrons and positrons with target atoms. This section describes the methods for computing DPA cross sections induced by electron and positron irradiation. The DPA cross section for an incident electron or positron can be calculated by

$$\sigma_{DPA}(E) = \int_0^{T_m} \upsilon(T)\frac{d\sigma}{dT}(E,T)dT \tag{1}$$

where E is the incident energy, T is the energy transferred to the target atom, $\upsilon(T)$ is the number of atomic displacements induced by an atom with energy T, $d\sigma/dT$ denotes the differential collision cross section, T_m is determined by

$$T_m(E) = \frac{2E}{Mc^2}(E + 2mc^2) \tag{2}$$

where Mc^2 and mc^2 respectively denote the rest energies of the target atom and an electron/positron.

2.1.1. Primary radiation damage model

The Norgett-Robinson-Torrens (NRT) model [17] is currently used as a standard for displacement damage quantification [18]. In the NRT formula, the number of Frenkel pairs is calculated by

$$\upsilon(T_a) = \begin{cases} 0, & T_a < E_d \\ 1, & E_d \le T_a < 2.5E_d \\ 0.8T_a/2E_d & T_a \ge 2.5E_d \end{cases} \tag{3}$$

where T_a is the so-called damage energy, E_d is the Threshold Displacement Energy (TDE). By interpreting Lindhard's numerical results [19], Robinson deduced an analytical formula as [20]

$$T_a(\varepsilon) = T/[1 + k_L(3.4008\varepsilon^{1/6} + 0.40244\varepsilon^{3/4} + \varepsilon)] \tag{4}$$

where $\varepsilon = T/E_L$ with $E_L = 86.931Z^{7/3}$ eV, $k_L = 0.133745Z^{2/3}A^{-1/2}$, A is the atomic mass number.

In fact, for a recoil atom with damage energy smaller than E_d but kinetic energy higher than E_d, it can be displaced [21]. The inelastic energy loss after its displacement does not influence the number of Frenkel pairs. Therefore, a modified-NRT (mNRT) formula is proposed by modifying the minimum threshold [21]

$$\upsilon(T) = \begin{cases} 0, & \boldsymbol{T < E_d} \\ 1, & \boldsymbol{E_d \le T \& } T_a(T) < 2.5E_d \\ 0.8T_a/2E_d & T_a(T) \ge 2.5E_d \end{cases} \tag{5}$$

The difference between the NRT and mNRT models is negligible for most cases but is shown to be important for the electron (similarly for positron and photon) irradiation-induced displacement damage cross section (e.g., for Fe shown in Fig. 1) [21]. Therefore, the mNRT model is recommended to compute the displacement damage cross sections in the present work. The threshold energy of electrons or positrons for displacing atoms is thus[1]

$$T_d^{e,p} = \sqrt{(mc^2)^2 + Mc^2E_d/2} - mc^2 \tag{6}$$

For obtaining results comparable with other evaluations of displacement damage, most values of TDE used in the present work are those recommended by ASTM [29]. The values and the corresponding references are summarized in Table 1. For Si, while the indirect measurements results in 20.5 ± 1.0 eV [30], density functional theory molecular dynamics simulations find 36 ± 3 eV [31]. These values are so different that the present work calculates the DPA cross sections using both values, even though the results displayed in the following figures are those using 20.5 eV.

2.1.2. Differential scattering cross section

Let θ denote the scattered angle of electron or positron in the center-of-mass frame. According to Eq. (11) in Ref. [34], one can obtain

$$\frac{T}{T_m} = \frac{1-\cos\theta}{2} = \sin^2\frac{\theta}{2} \tag{7}$$

Therefore, the Mott differential scattering cross section [35,36] can be reformulated as

$$\frac{d\sigma}{dT}(E,T) = \frac{d\sigma^{Ruth}}{dT}(E,T)\mathscr{R}^{Mott}(E,T) \tag{8}$$

where $d\sigma^{Ruth}/dT$ is the Rutherford cross section

$$\frac{d\sigma^{Ruth}}{dT}(E,T) = \frac{\pi Z^2(k_Ce^2)^2(1-\beta^2)T_m}{(mc^2)^2\beta^4T^2} \tag{9}$$

where $k_C \approx 8.988 \times 10^9 \mathrm{N \bullet m^2 \bullet C^{-2}}$ is the Coulomb constant, $mc^2 \approx 0.511$ MeV is the rest energy of the electron or positron, β is the ratio of initial electron speed to the speed of light (i.e., $\beta^2 = E(E+2mc^2)/(E+mc^2)^2$), Z is the atomic number. The Mott ratio $\mathscr{R}^{Mott}$ can be reformulated by [36]

[1] The present work still uses the conventional hypothesis that the displacement probability is a step function (i.e., 0 below TDE and 1 otherwise). The lattice direction-dependent TDE [22], the subsequent strictly increasing continuous displacement function in the vicinity of TDE [1,23,24], and the thermal vibration of targets [25,26] influence the damage cross section for energy around $T_d^{e,p}$. Such influence is limited for high recoil energies (e.g., the atomic vibration for neutron [27] and electron [28] irradiation) and not emphasized in the present study.

Table 1
TDE values for the monatomic materials studied in the present work.

	Li	C	O	Al	Si	Cr	Fe	Ni	Cu	W	U
Z	3	6	8	13	14	24	26	28	29	74	92
E_d (eV)	20	30	20	25	20.5	40	40	40	30	90	40
Ref.	[32]	[33]	*	[29]	[30]	[29]	[29]	[29]	[29]	[29]	[32]

* O is included because it exists in many polyatomic materials. 20 eV is an estimation.

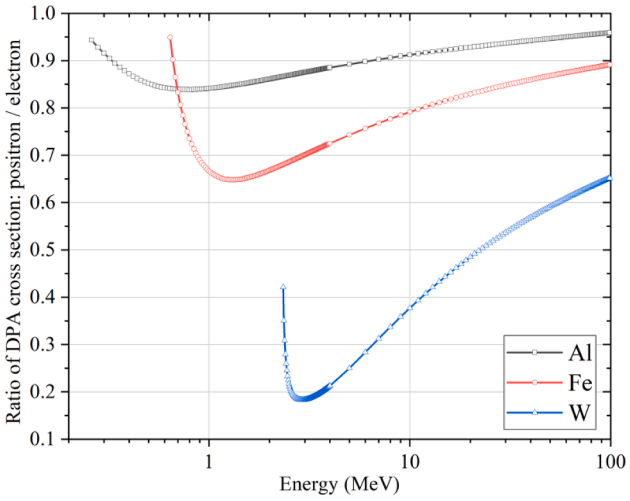

Fig. 2. Ratio of positron-induced DPA cross sections to those induced by electron for Al, Fe, and W.

$$\mathscr{R}^{Mott}(E,T)=\frac{4T}{T_m\gamma^2}|F|^2+\frac{2\beta^2(mc)^2T^2}{(\alpha Z)^2(T_m-T)^2}|G|^2 \tag{10}$$

where $\gamma=1+E/mc^2$ is the Lorentz factor, $\alpha\approx1/137.036$ is the fine structure constant, and the complex functions F and G can be directly calculated with the equations given in Ref. [36] by using Eq. (7). **It is noted that Z in Ref. [36] should be replaced by $-Z$ for computing the Mott ratio for positron**. Therefore, as the ratios shown in Fig. 2, the positron-induced DPA cross sections are different from the electron-induced ones.

Fig. 3 compares the DPA cross sections computed with the McKinley-Feshbach approximation and Mott cross section for aluminum (Al), iron (Fe), and tungsten (W). In general, the McKinley-Feshbach model can give reliable displacement damage cross sections for light atoms. However, as explained above, the McKinley-Feshbach analytical formula for electron and positron scattering is not valid for Z > 27. Taking tungsten (Z = 74) as an example, the use of the McKinley-Feshbach formula leads to a 10 %-60 % underestimation of DPA cross section for both electron and positron irradiation. Consequently, the accurate Mott cross section is recommended for general displacement damage evaluation.

2.2. Stopping powers for electron and positron

Since the photo-atomic interactions induce radiation damage through the two products: electrons and positrons, their losses of energy in matter (quantified by the so-called stopping powers) are required for computing photo-atomic radiation damage (to be shown in Section 2.3). Various stopping power formulae have been compared in Ref. [15]. Because the stopping powers compiled in the International Commission on Radiation Unit and measurements (ICRU) [37] are almost state-of-the-art data, these data are used in the present work. For isotopes without available stopping powers for positron in the ICRU, the stopping powers are deduced with the compiled data and the semi-empirical formulae given in the ICRU report and summarized here.

For both electron and positron, the total stopping power is constituted by the collision and radiative stopping powers

$$S(E)=S^c(E)+S^r(E) \tag{11}$$

where the subscripts c and r represent collision and radiative, respectively. As the examples shown in Fig. 4, the ratio of collision stopping power for the positron to that for the electron is not sensitive to the target material for the collision stopping power. Therefore, in the case where the stopping power for positron in monatomic materials x is not directly recommended in the ICRU report, the collision stopping power for positron $\left[S_p^c(E)\right]_x$ is calculated by

$$\left[S_p^c(E)\right]_x\approx\left[S_e^c(E)\right]_x\times\left[\frac{S_p^c(E)}{S_e^c(E)}\right]_y \tag{12}$$

where the subscripts p and e respectively denote positron and electron, y is chosen for its atomic number as close as possible to that of x and its collision stopping powers for both electron and positron are given in the ICRU report. In the present work, linear interpolation on the two nearest neighbor elements is used.

For the radiative stopping power, according to Ref. [37], one can imply that

$$\frac{S_p^r(E)}{S_e^r(E)}\approx\eta\left(E/Z^2\right) \tag{13}$$

where S_e^r and S_p^r are respectively the radiative stopping powers for electron and positron, η is the ratio of energy loss due to the interaction of positron with the atomic nucleus to that of electron with the nucleus. η depends only on E/Z^2 and is shown in Fig. 5 [37]. Therefore, in the case of no available data, the radiative stopping power for positron in a specific monatomic material x is calculated by

$$\left[S_p^r(E)\right]_x\approx\left[S_e^r(E)\right]_x\times\eta\left(E/Z_x^2\right) \tag{14}$$

According to Eq. (13), one can also calculate $\left[S_p^r(E)\right]_x$ using η deduced from a specific target y by

$$\left[S_p^r(E)\right]_x\approx\left[S_e^r(E)\right]_x\times\left[\frac{S_p^r(E')}{S_e^r(E')}\right]_y \tag{15}$$

where y is chosen for its atomic number as close as possible to that of x, and

$$E'=EZ_y^2/Z_x^2 \tag{16}$$

Fig. 6 shows the total mass stopping powers for electron and positron in Al, Fe, and W.

2.3. Photon irradiation-induced displacement cross sections

The total DPA cross section induced by photo-atomic interactions is

$$\sigma_{DPA}(E_\gamma)=\sigma_{DPA}^{PE}(E_\gamma)+\sigma_{DPA}^{CS}(E_\gamma)+\sigma_{DPA}^{PP}(E_\gamma) \tag{17}$$

where σ_{DPA}^{PE} σ_{DPA}^{CS}, and σ_{DPA}^{PP} represent the DPA cross sections induced by the PE, CS, and PP, respectively. The contributions of PE and CS can be calculated with the methods recommended in our previous work [15].

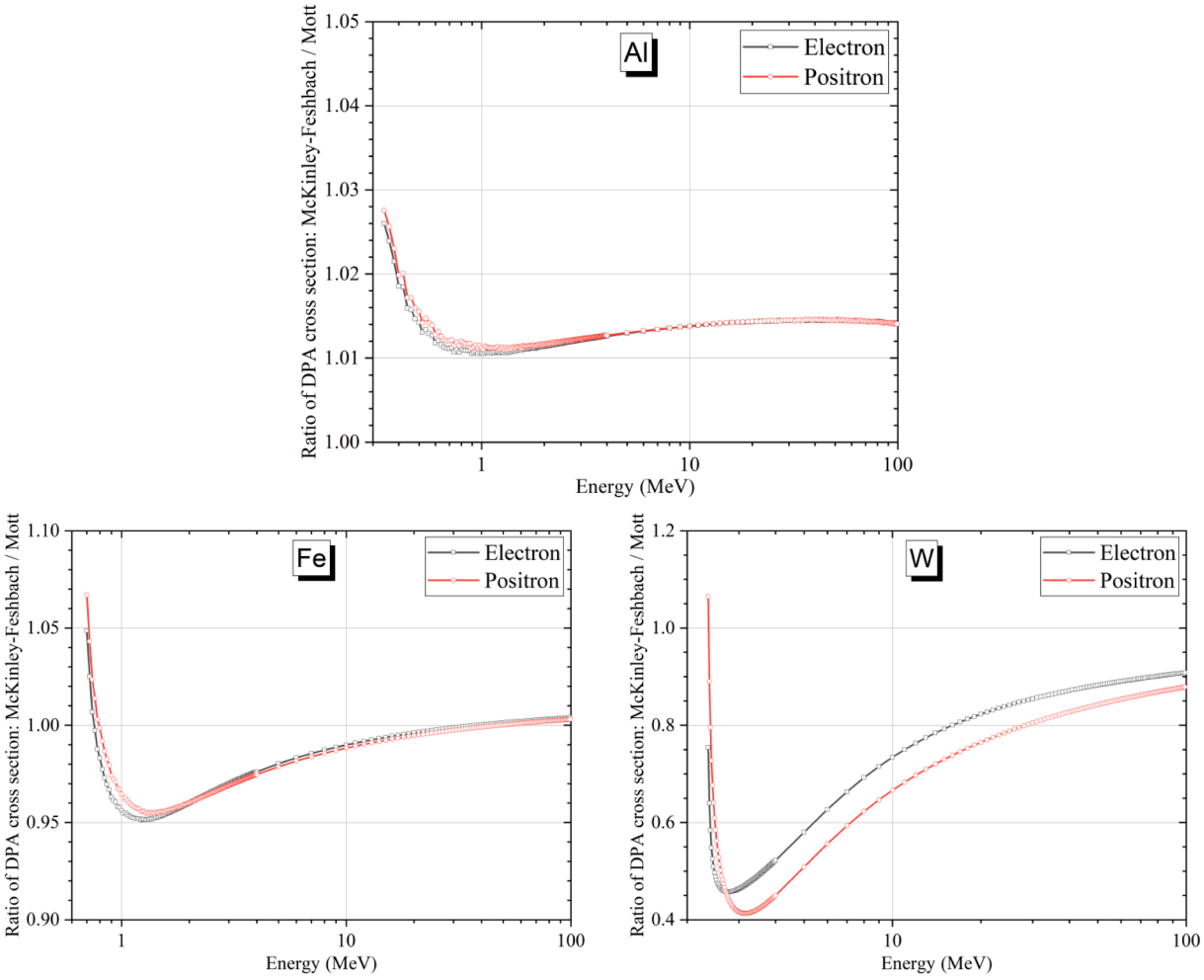

Fig. 3. Ratio of DPA cross sections computed with the McKinley-Feshbach approach to Mott series for Al, Fe, and W.

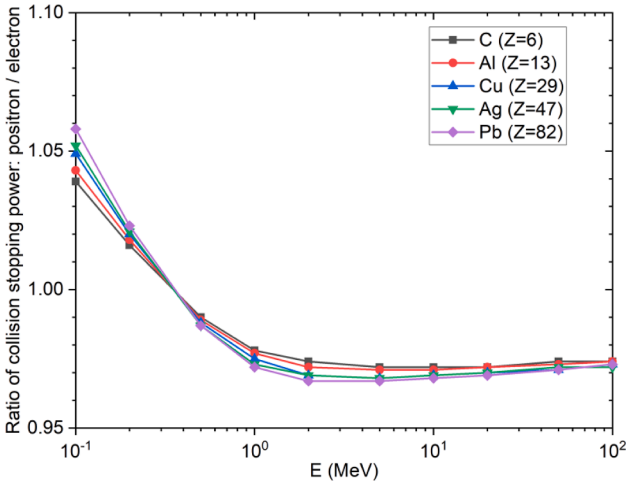

Fig. 4. Ratio of collision stopping power for positron to that for electron.

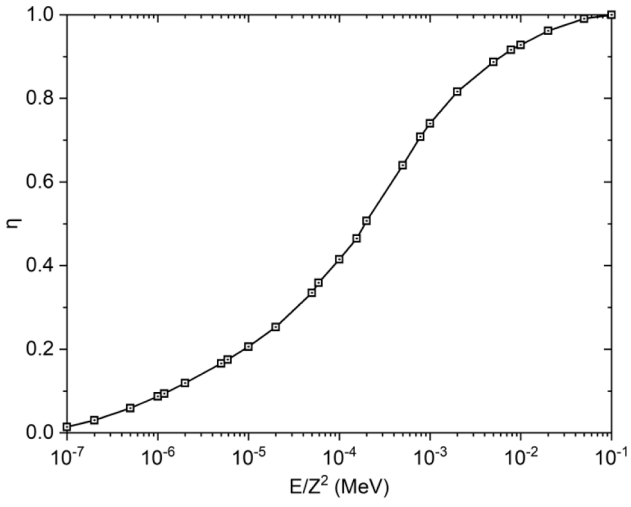

Fig. 5. Ratio of energy loss by positron-nucleus interaction to that by electron-nucleus interaction (data from Ref. [37]).

The required binding energies for the PE can be found in Ref. [38]. The K-shell binding energies for H ($Z = 1$) to U ($Z = 92$) reevaluated by Bearden and Burr [38] are plotted in Fig. 7. In general, the binding energies are negligible for displacement damage calculation because they are smaller than 116 keV for $Z \leq 92$. The present work mainly proposes an accurate method for calculating the DPA cross section induced by the PP.

The PP-induced displacement damage cross section is calculated by

$$\sigma_{DPA}^{PP}(E_\gamma) = \int_{mc^2}^{E_\gamma - mc^2} \frac{d\sigma^{PP}(E_\gamma, E)}{dE} \left[n_e(E_\gamma - E - mc^2) + n_p(E - mc^2) \right] dE \tag{18}$$

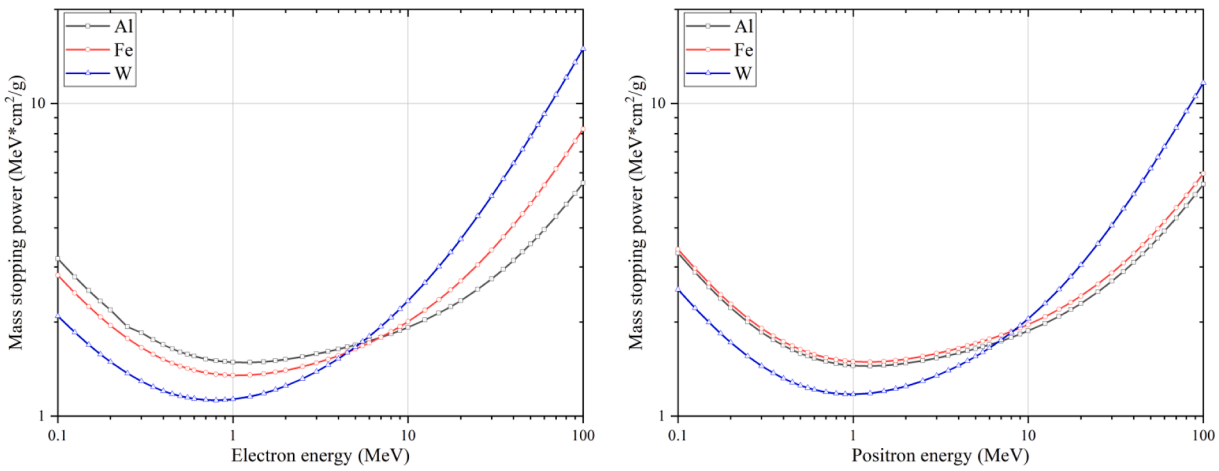

Fig. 6. Mass stopping power for electron (left) and positron (right) in Al, Fe, and W.

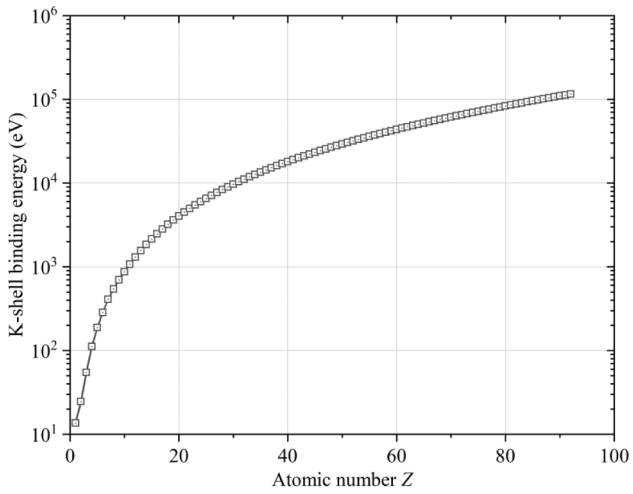

Fig. 7. K-shell binding energy for atoms from H to U (data from Ref. [38]).

where $d\sigma^{PP}(E_\gamma, E)/dE$ is the differential cross section for a photon with an energy of E_γ producing an electron–positron pair with the kinetic energy of the positron being E, $n_e(E)$ and $n_p(E)$ respectively denote the average number of atom displacements induced by an electron and a positron with kinetic energy E. $n_i(E)$ $(i = e,p)$ is calculated using the DPA cross sections σ^i_{DPA} (Section 2.1) and stopping powers S_i (Section 2.2)

$$n_i(E) = N_V \int_0^E \frac{\sigma^i_{DPA}(T)}{S_i(T)} dT, i = e, p \tag{19}$$

where N_V is the atomic density of the material.

For simplifying the expression, let denote $\mathscr{E} = E_\gamma - E$ for the total energy of the positron from the PP. The differential cross section $d\sigma^{PP}/dE$ derived by Bethe and Heitler [39,40] is

$$\begin{aligned}\frac{d\sigma^{PP}(E_\gamma, E)}{dE} = {} & \frac{\alpha Z^2 (k_C e^2)^2}{(mc^2)^2 E_\gamma^3} p_+ p_- \left\{ -\frac{4}{3} - 2E\mathscr{E}\frac{p_+^2 + p_-^2}{p_+^2 p_-^2} + (mc^2)^2 \left(\frac{\mathscr{E}\epsilon_-}{p_-^3} \right.\right. \\ & \left. + \frac{E\epsilon_+}{p_+^3} - \frac{\epsilon_+ \epsilon_-}{p_+ p_-} \right) + L \left[\frac{E_\gamma^2}{p_+^3 p_-^3} \left(E^2\mathscr{E}^2 + p_+^2 p_-^2 \right) \right. \\ & \left. - \frac{8}{3}\frac{E\mathscr{E}}{p_+ p_-} \right] - \frac{(mc^2)^2 E_\gamma}{2p_+ p_-} \left(\frac{E\mathscr{E} - p_-^2}{p_-^3}\epsilon_- + \frac{E\mathscr{E} - p_+^2}{p_+^3}\epsilon_+ \right. \\ & \left.\left. + \frac{2E_\gamma E\mathscr{E}}{p_+^2 p_-^2} \right) \right\}\end{aligned} \tag{20}$$

where

Table 2
Values of $c(\zeta)$ [39].

ζ	2	2.5	3	4	5	6	8	10	15
$c(\zeta)$	0.21	0.16	0.13	0.09	0.065	0.05	0.03	0.02	0.01

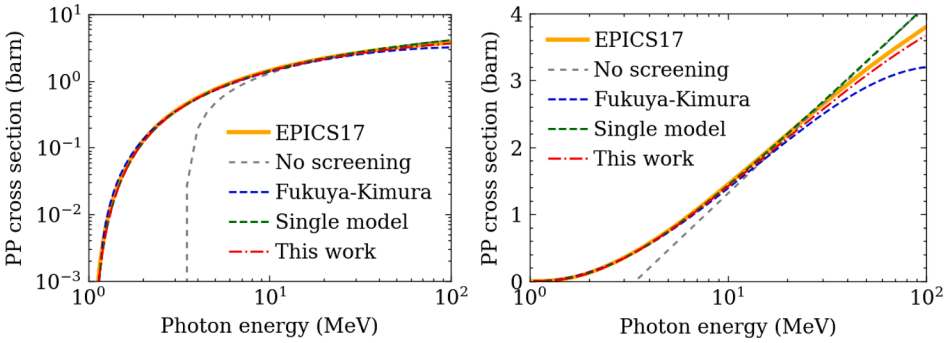

Fig. 8. Integral PP cross sections in Fe (left: logarithmic y-axis, right: linear y-axis). Single model refers to the results using the single model described by Eq. (20).

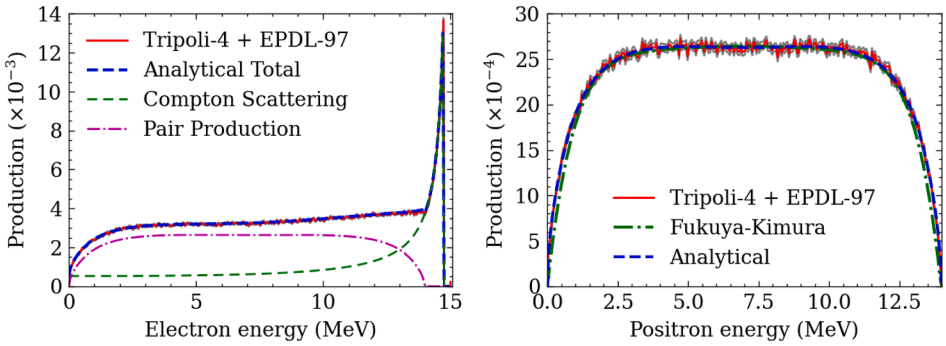

Fig. 9. Electron (left) and positron (right) productions of a 15 MeV photon in Fe.

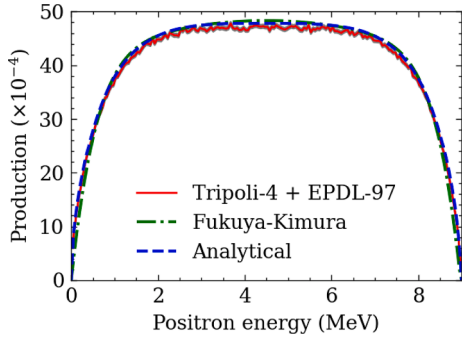

Fig. 10. Positron production of a 10 MeV photon in W.

$$
\begin{aligned}
p_+ &= \left(\mathscr{E}^2 - (mc^2)^2\right)^{1/2} \\
p_- &= \left(E^2 - (mc^2)^2\right)^{1/2} \\
\epsilon_+ &= 2\ln\left[(\mathscr{E} + p_+)/mc^2\right] \\
\epsilon_- &= 2\ln\left[(E + p_-)/mc^2\right] \\
L &= 2\ln\left[\left(E\mathscr{E} + p_+p_- + (mc^2)^2\right)\Big/\left(E_\gamma mc^2\right)\right]
\end{aligned}
\tag{21}
$$

The above model, i.e., Eq. (20), is however not physically valid for high photon energy. For $E_\gamma > 10mc^2$, let define the variable

$$
\zeta = 100\frac{mc^2E_\gamma}{E\mathscr{E}Z^{1/3}} \tag{22}
$$

If $0 \le \zeta \le 2$, the differential PP cross section is [39]

$$
\frac{d\sigma^{PP}(E_\gamma, E)}{dE} = \frac{\alpha Z^2(k_Ce^2)^2}{(mc^2)^2E_\gamma^3}\left\{\left(E^2 + \mathscr{E}^2\right)\left[\varphi_1(\zeta) - \frac{4}{3}\ln(Z)\right] + \frac{2}{3}E\mathscr{E}\left[\varphi_2(\zeta) - \frac{4}{3}\ln(Z)\right]\right\} \tag{23}
$$

where φ_1 and φ_2 are two functions constrained by [39,41]

$$
\begin{cases}
\varphi_1(0) = 4\ln(183) \approx 20.84 \\
\varphi_2(0) = \varphi_1(0) - \dfrac{2}{3} \approx 20.17
\end{cases}
\tag{24}
$$

and can be approached by the following analytical expressions

$$
\begin{cases}
\varphi_1(\zeta) = 20.84 - 4.4098\zeta + 1.3187\zeta^2 - 0.2074\zeta^3 \\
\varphi_2(\zeta) = \begin{cases} 20.17 - 2.1903\zeta - 1.6074\zeta^2 + 1.1590\zeta^3 & \zeta \le 1 \\ \varphi_1(\zeta) & \zeta > 1 \end{cases}
\end{cases}
\tag{25}
$$

For $2 < \zeta \le 15$, Bethe and Heitler [39] proposed a more convenient formula rather than Eq. (23) for computing $d\sigma^{PP}/dE$

$$
\frac{d\sigma^{PP}(E_\gamma, E)}{dE} = 4\frac{\alpha Z^2(k_Ce^2)^2}{(mc^2)^2E_\gamma^3}\left(E^2 + \mathscr{E}^2 + \frac{2}{3}E\mathscr{E}\right)\left[\ln\left(\frac{2E\mathscr{E}}{mc^2E_\gamma}\right) - \frac{1}{2} - c(\zeta)\right] \tag{26}
$$

where $c(\zeta)$ is tabulated in Table 2. When $\zeta > 15$, the model Eq. (20) is applied.

The integral cross sections of PP for Fe are compared in Fig. 8. Good agreement with EPICS2017 [42] is observed. It is also observed that the total PP cross section computed using the models presented in the present work is better than the approach proposed by Fukuya and Kimura [13] when $E_\gamma > 20$ MeV. Even though the use of single model (20) (or Eqs. (23) and (25)) is not so adequate for high photon energy, as explained above, Eq. (20) vs. Eqs. (23) and (25) lead to close results. However, for rigorous consideration, the combined model using Eqs. (20), (23), and (25) is applied in the present study. It is also noticeable that the screening effect is not negligible.

Because the differential cross section is used for computing displacement damage cross section, we compare the electron and positron production spectra with other methods. The positron spectrum in Fe induced by a 15 MeV photon and that in W induced by a 10 MeV photon are shown in Fig. 9 and Fig. 10, respectively. Because the positrons are produced only from the PP, the good agreement between analytical calculations and Monte Carlo simulations (Tripoli-4 [43]) using the Evaluated Photon Data Library (EPDL)-97 [44] numerically validates the accuracy of using Eqs. (20), (23), and (25) for computing the differential scattering cross sections of PP. In addition, the use of Eqs. (20), (23), and (25) for the PP, the Klein-Nishina formula [45] for the CS, and the Hall formula [40,46] for the PE results in the electron spectrum in good agreement with EPDL-97 (e.g., the example shown in Fig. 9). The agreement with Monte Carlo simulations is also improved when compared with the Fukuya-Kimura approach for iron [13]. Thereby, the application of Eqs. (20), (23), and (25) for calculating displacement damage cross sections induced by the PP is again numerically justified.

3. Results and discussion

3.1. DPA cross sections by electron and positron irradiation

Fig. 11 plots the electron-induced DPA cross sections in some selected monatomic materials. The corresponding DPA cross sections induced by positron irradiation are shown in Fig. 12. The data are tabulated in a coarser energy grid in Table 3 for simpler utilization. For an intuitive comparison, Fig. 13 illustrates the ratios of positron-induced DPA cross sections to the electron-induced ones. In general, the difference between the electron and positron-induced DPA cross sections increases with increasing atomic number, consistent with Oen's observation [47]. The minimum ratios are smaller than 0.2 for W and U. However, it has not been indicated that the positron-induced

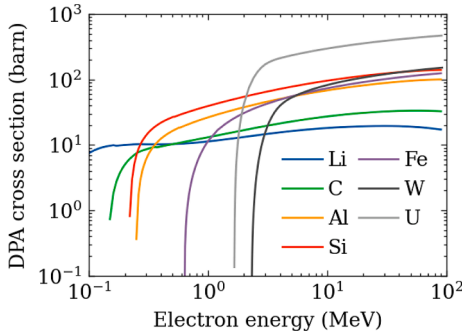

Fig. 11. Electron-induced DPA cross sections in various elementary materials.

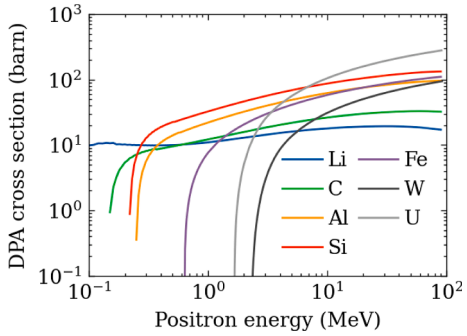

Fig. 12. Positron-induced DPA cross sections in various elementary materials.

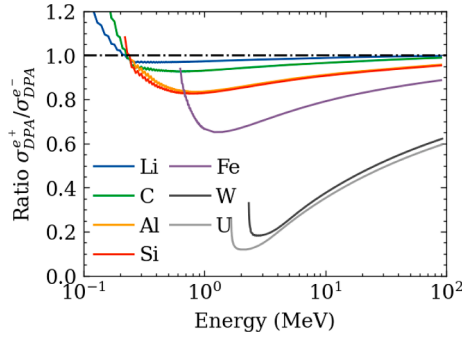

Fig. 13. Ratios of positron-induced DPA cross sections to those induced by electron in various elementary materials.

displacement damage cross section could be larger than the electron-induced one for small atomic numbers at relatively low energies, as shown in Fig. 13.

3.2. DPA cross sections by photon irradiation

Fig. 14 shows the total photon-induced DPA cross sections for Fe determined in previous works [12,13,15] and that calculated with the methods proposed in the present work. For intuitive comparison, Fig. 15 illustrates the ratios of previous DPA cross sections to the ones of the present calculation. As analyzed in Ref. [15], Kwon and Motta [12] evidently overestimated the photon-induced DPA cross section for photon energy between 2 and 10 MeV. It is noted that the numerical accuracy of the present work is slightly improved when compared with our previous work [15] for photon energy comparable with mc^2.

The differences between Refs. [13,15] and the present calculation for photon energy above 3 MeV is mainly due to the difference between the NRT and mNRT models. The latter is larger than the former when $E_d \leq T\&T_a(T) < E_d$. In addition, different reaction models are used: (1) McKinley-Feshbach approximation in Refs. [13,15] vs. accurate Mott cross section in the present work; (2) the Fukuya-Kimura analytical approach in Refs. [13,15] vs. the present combined model for the differential cross section of PP. For the first source, the difference is already observed between DPA cross sections computed by using the McKinley-Feshbach approach and by using the accurate Mott cross section for Fe (Fig. 3), of which Z = 26, within but close to the limit of the applicative range of the McKinley-Feshbach approximation (Z < 27.4 [16]).

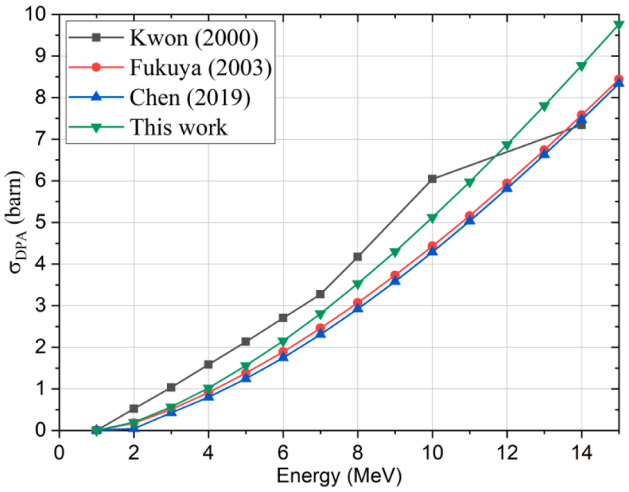

Fig. 14. Photon-induced DPA cross sections for Fe from different calculations: Kwon (2000) [12], Fukuya (2003) [13], Chen (2019) [15], and this work.

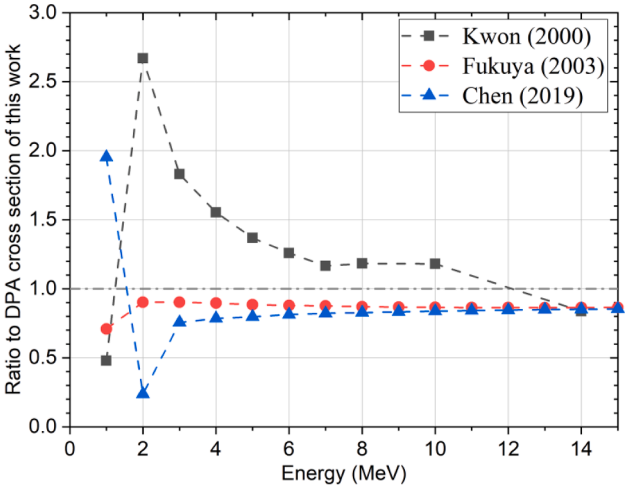

Fig. 15. Ratios of previous photon-induced DPA cross sections (cf. Fig. 14 and Refs. [12,13,15]) to the one obtained in the present work.

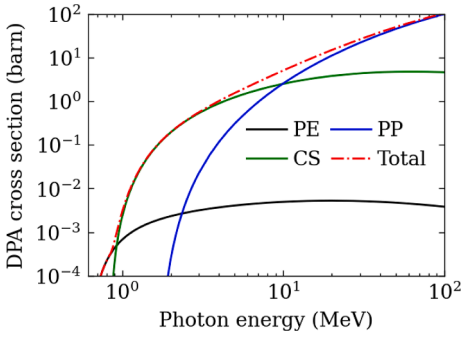

Fig. 16. Photon-induced DPA cross sections for Fe calculated with the methods proposed in the present work.

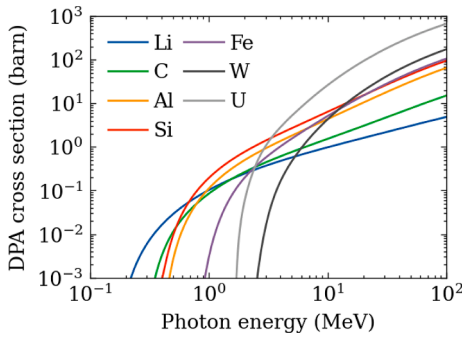

Fig. 17. Photon-induced DPA cross sections for various elements (from Li to U).

Therefore, the Mott cross section should be used for atoms heavier than Fe.

The present work calculates photon-induced DPA cross sections for incident energy up to 100 MeV since some applications (e.g., Ref. [8]) need energy beyond the current limits (20 MeV or even lower). The photon-induced DPA cross sections by the CS, PE, and PP as well as the total displacement cross sections for Fe are shown in Fig. 16 with photon energy up to 100 MeV. Similar plots for Li and U are displayed in Fig. 18 in Appendix for providing more general information on the contribution and trend of each reaction. Fig. 17 shows the total photon-induced DPA cross sections for various selected elements. For the application purpose, the DPA cross sections by electron, proton, and photon irradiations are tabulated in Table 3 in Appendix. These data can be directly used to compute photon irradiation damage by folding with the photon spectra in specific materials in any radiation environment.

4. Summary

The present work proposes more rigorous methods for calculating electron, positron, and photon irradiation-induced displacement damage cross sections. Compared with previous works, the main improvements are:

- Accurate Mott scattering cross sections are used for both electron and positron (especially important for heavy atoms);
- Rigorous methods for computing stopping powers based on the recommendation given by ICRU are used for both electron and positron;
- Rigorous differential cross section of PP is applied by combining three semi-analytical models;
- The atomic displacements induced by recoil energy T in the range of $E_d \leq T \& T_a(T) < E_d$ is taken into account.

The displacement cross sections for incident energy up to 100 MeV are calculated for various monatomic materials using the proposed methods. The photon-induced displacement damage cross sections obtained in the present work are slightly larger than the previous calculations, thus enhancing the contribution of photon irradiation-induced displacement damage. All the displacement damage cross sections are tabulated in Appendix so that they can be easily used by other researchers.

CRediT authorship contribution statement

Shengli Chen: Conceptualization, Methodology, Validation, Investigation, Writing – review & editing, Funding acquisition, Software, Formal analysis, Writing – original draft, Visualization, Data curation, Project administration. **Dingbang Cai:** Validation, Investigation, Software, Formal analysis, Visualization, Data curation. **David Bernard:** Formal analysis, Writing – review & editing. **Yannick Peneliau:** Methodology, Software, Writing – review & editing.

Declaration of Competing Interest

The authors declare that they have no known competing financial interests or personal relationships that could have appeared to influence the work reported in this paper.

Data availability

Data are given in Appendix

Acknowledgments

S. Chen acknowledges the support from the National Natural Science Foundation of China (under Grant No. 12205390& 12105377), Guangdong Major Project of Basic and Applied Basic Research (under Grant No. 2021B0301030006), and Guangdong Basic and Applied Basic Research Foundation (under Grant No. 2019A1515010849).

Appendix

Fig. 18 displays the photon-induced DPA cross sections for Li and U, two elements having respectively the lowest and highest atomic numbers in the present study. Table 3 lists the digital data for electron, positron, and photon-induced DPA cross section. It should be noted that the present data are consistent with the nuclei (e.g., neutron and proton) and ions irradiation damage quantified by the current practice standard. The athermal recombination of displaced atoms [32,48,49] is not yet included.

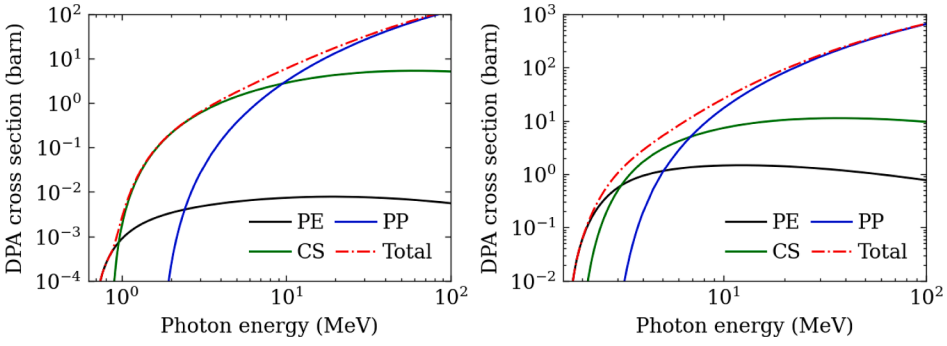

Fig. 18. Photon-induced DPA cross sections for Li (left) and U (right).

Table 3
DPA cross sections (in barn) induced by electron, positron, and photon for various monatomic materials.

	Li			C		
E (MeV)	Electron	Positron	Photon	Electron	Positron	Photon
0.1	7.49e+0	9.82e+0	4.02e-6	0	0	0
0.3	1.02e+1	9.91e+0	5.87e-3	8.54e+0	8.10e+0	6.46e-5
0.5	1.03e+1	9.97e+0	2.88e-2	1.02e+1	9.52e+0	1.12e-2
0.6	1.04e+1	1.01e+1	4.29e-2	1.09e+1	1.01e+1	2.28e-2
0.7	1.06e+1	1.03e+1	5.76e-2	1.15e+1	1.07e+1	3.65e-2
0.8	1.09e+1	1.05e+1	7.26e-2	1.21e+1	1.12e+1	5.17e-2
0.9	1.11e+1	1.08e+1	8.77e-2	1.26e+1	1.17e+1	6.79e-2
1.0	1.13e+1	1.10e+1	1.03e-1	1.31e+1	1.22e+1	8.49e-2
1.5	1.23e+1	1.20e+1	1.76e-1	1.52e+1	1.42e+1	1.74e-1
2.0	1.32e+1	1.29e+1	2.45e-1	1.68e+1	1.59e+1	2.65e-1
2.5	1.40e+1	1.37e+1	3.08e-1	1.82e+1	1.72e+1	3.54e-1
3.0	1.46e+1	1.43e+1	3.68e-1	1.94e+1	1.84e+1	4.40e-1
4.0	1.55e+1	1.53e+1	4.77e-1	2.13e+1	2.03e+1	6.08e-1
5.0	1.63e+1	1.60e+1	5.75e-1	2.28e+1	2.18e+1	7.69e-1
6.0	1.68e+1	1.66e+1	6.66e-1	2.40e+1	2.30e+1	9.26e-1
7.0	1.73e+1	1.70e+1	7.51e-1	2.50e+1	2.40e+1	1.08e+0
8.0	1.76e+1	1.74e+1	8.32e-1	2.59e+1	2.49e+1	1.23e+0
9.0	1.79e+1	1.77e+1	9.08e-1	2.66e+1	2.57e+1	1.38e+0
10	1.82e+1	1.79e+1	9.81e-1	2.72e+1	2.63e+1	1.53e+0
12	1.85e+1	1.83e+1	1.12e+0	2.83e+1	2.74e+1	1.83e+0
14	1.88e+1	1.86e+1	1.25e+0	2.91e+1	2.83e+1	2.13e+0
16	1.90e+1	1.88e+1	1.38e+0	2.98e+1	2.90e+1	2.43e+0
18	1.91e+1	1.90e+1	1.49e+0	3.04e+1	2.96e+1	2.73e+0
20	1.93e+1	1.91e+1	1.61e+0	3.09e+1	3.01e+1	3.04e+0
25	1.94e+1	1.93e+1	1.88e+0	3.18e+1	3.10e+1	3.80e+0
30	1.95e+1	1.94e+1	2.14e+0	3.24e+1	3.17e+1	4.58e+0
35	1.95e+1	1.94e+1	2.38e+0	3.28e+1	3.21e+1	5.35e+0
40	1.94e+1	1.93e+1	2.62e+0	3.31e+1	3.25e+1	6.13e+0
45	1.92e+1	1.91e+1	2.84e+0	3.33e+1	3.27e+1	6.91e+0
50	1.90e+1	1.89e+1	3.06e+0	3.34e+1	3.28e+1	7.69e+0
60	1.86e+1	1.85e+1	3.46e+0	3.34e+1	3.29e+1	9.23e+0
70	1.81e+1	1.81e+1	3.85e+0	3.33e+1	3.28e+1	1.07e+1
80	1.77e+1	1.76e+1	4.21e+0	3.30e+1	3.26e+1	1.22e+1
90	1.72e+1	1.71e+1	4.55e+0	3.27e+1	3.23e+1	1.37e+1
100	1.72e+1	1.71e+1	4.87e+0	3.27e+1	3.23e+1	1.51e+1
	O			Al		
E (MeV)	Electron	Positron	Photon	Electron	Positron	Photon
0.2	1.33e+1	1.39e+1	9.11e-5	0	0	0
0.3	1.95e+1	1.81e+1	6.24e-4	5.89e+0	5.56e+0	6.56e-5
0.5	2.25e+1	2.05e+1	3.07e-2	1.63e+1	1.40e+1	2.56e-3
0.6	2.39e+1	2.16e+1	5.82e-2	1.88e+1	1.59e+1	1.25e-2
0.7	2.50e+1	2.27e+1	8.99e-2	2.11e+1	1.77e+1	2.97e-2
0.8	2.62e+1	2.37e+1	1.25e-1	2.31e+1	1.93e+1	5.28e-2
0.9	2.72e+1	2.47e+1	1.61e-1	2.48e+1	2.07e+1	8.03e-2
1.0	2.82e+1	2.56e+1	1.99e-1	2.64e+1	2.21e+1	1.11e-1
1.5	3.24e+1	2.97e+1	3.97e-1	3.28e+1	2.78e+1	2.94e-1
2.0	3.58e+1	3.31e+1	5.95e-1	3.77e+1	3.23e+1	4.98e-1
2.5	3.87e+1	3.59e+1	7.91e-1	4.17e+1	3.61e+1	7.09e-1
3.0	4.11e+1	3.83e+1	9.83e-1	4.50e+1	3.93e+1	9.24e-1
4.0	4.51e+1	4.23e+1	1.36e+0	5.05e+1	4.46e+1	1.37e+0
5.0	4.83e+1	4.55e+1	1.73e+0	5.48e+1	4.88e+1	1.82e+0
6.0	5.09e+1	4.81e+1	2.10e+0	5.83e+1	5.23e+1	2.29e+0
7.0	5.31e+1	5.03e+1	2.47e+0	6.14e+1	5.53e+1	2.78e+0
8.0	5.49e+1	5.22e+1	2.85e+0	6.40e+1	5.79e+1	3.29e+0
9.0	5.66e+1	5.38e+1	3.22e+0	6.63e+1	6.02e+1	3.81e+0
10	5.80e+1	5.53e+1	3.60e+0	6.83e+1	6.23e+1	4.35e+0
12	6.05e+1	5.78e+1	4.36e+0	7.18e+1	6.58e+1	5.47e+0
14	6.25e+1	5.98e+1	5.13e+0	7.47e+1	6.88e+1	6.65e+0
16	6.41e+1	6.15e+1	5.91e+0	7.72e+1	7.13e+1	7.87e+0
18	6.55e+1	6.30e+1	6.69e+0	7.94e+1	7.35e+1	9.12e+0
20	6.67e+1	6.42e+1	7.48e+0	8.13e+1	7.54e+1	1.04e+1
25	6.91e+1	6.67e+1	9.45e+0	8.51e+1	7.94e+1	1.37e+1
30	7.08e+1	6.85e+1	1.14e+1	8.82e+1	8.26e+1	1.72e+1
35	7.20e+1	6.99e+1	1.34e+1	9.06e+1	8.51e+1	2.07e+1
40	7.29e+1	7.09e+1	1.53e+1	9.26e+1	8.72e+1	2.43e+1
45	7.36e+1	7.16e+1	1.73e+1	9.42e+1	8.90e+1	2.78e+1
50	7.40e+1	7.21e+1	1.91e+1	9.57e+1	9.05e+1	3.14e+1
60	7.43e+1	7.26e+1	2.29e+1	9.79e+1	9.30e+1	3.85e+1
70	7.42e+1	7.26e+1	2.64e+1	9.96e+1	9.49e+1	4.55e+1
80	7.38e+1	7.23e+1	2.98e+1	1.01e+2	9.65e+1	5.23e+1
90	7.32e+1	7.18e+1	3.31e+1	1.02e+2	9.77e+1	5.88e+1
100	7.32e+1	7.18e+1	3.62e+1	1.02e+2	9.77e+1	6.52e+1

	Si (20.5 eV)			Si (36 eV)		
E (MeV)	Electron	Positron	Photon	Electron	Positron	Photon
0.3	1.38e+1	1.27e+1	3.38e-4	0	0	0
0.5	2.65e+1	2.24e+1	9.22e-3	6.39e+0	5.56e+0	7.40e-5
0.6	2.96e+1	2.46e+1	3.03e-2	9.17e+0	7.70e+0	7.96e-4
0.7	3.24e+1	2.69e+1	6.17e-2	1.14e+1	9.39e+0	4.88e-3
0.8	3.50e+1	2.89e+1	1.01e-1	1.30e+1	1.06e+1	1.30e-2
0.9	3.73e+1	3.09e+1	1.45e-1	1.45e+1	1.18e+1	2.48e-2
1.0	3.94e+1	3.27e+1	1.94e-1	1.59e+1	1.30e+1	3.99e-2
1.5	4.79e+1	4.03e+1	4.72e-1	2.13e+1	1.75e+1	1.45e-1
2.0	5.45e+1	4.64e+1	7.73e-1	2.53e+1	2.11e+1	2.75e-1
2.5	5.98e+1	5.15e+1	1.08e+0	2.85e+1	2.40e+1	4.15e-1
3.0	6.44e+1	5.58e+1	1.39e+0	3.11e+1	2.66e+1	5.62e-1
4.0	7.18e+1	6.30e+1	2.03e+0	3.54e+1	3.07e+1	8.71e-1
5.0	7.76e+1	6.88e+1	2.70e+0	3.88e+1	3.39e+1	1.19e+0
6.0	8.24e+1	7.36e+1	3.38e+0	4.16e+1	3.67e+1	1.53e+0
7.0	8.65e+1	7.76e+1	4.10e+0	4.39e+1	3.90e+1	1.89e+0
8.0	9.01e+1	8.12e+1	4.84e+0	4.60e+1	4.10e+1	2.26e+0
9.0	9.32e+1	8.43e+1	5.61e+0	4.78e+1	4.28e+1	2.64e+0
10	9.60e+1	8.71e+1	6.40e+0	4.93e+1	4.44e+1	3.04e+0
12	1.01e+2	9.19e+1	8.05e+0	5.21e+1	4.71e+1	3.87e+0
14	1.05e+2	9.59e+1	9.78e+0	5.44e+1	4.94e+1	4.74e+0
16	1.08e+2	9.94e+1	1.16e+1	5.63e+1	5.14e+1	5.66e+0
18	1.11e+2	1.02e+2	1.34e+1	5.80e+1	5.31e+1	6.60e+0
20	1.14e+2	1.05e+2	1.53e+1	5.95e+1	5.46e+1	7.57e+0
25	1.19e+2	1.11e+2	2.02e+1	6.25e+1	5.77e+1	1.01e+1
30	1.23e+2	1.15e+2	2.53e+1	6.49e+1	6.02e+1	1.27e+1
35	1.27e+2	1.18e+2	3.05e+1	6.68e+1	6.22e+1	1.54e+1
40	1.29e+2	1.21e+2	3.57e+1	6.84e+1	6.39e+1	1.81e+1
45	1.32e+2	1.24e+2	4.09e+1	6.97e+1	6.53e+1	2.08e+1
50	1.33e+2	1.26e+2	4.62e+1	7.08e+1	6.65e+1	2.36e+1
60	1.36e+2	1.29e+2	5.66e+1	7.26e+1	6.85e+1	2.90e+1
70	1.38e+2	1.31e+2	6.67e+1	7.39e+1	6.99e+1	3.43e+1
80	1.39e+2	1.33e+2	7.65e+1	7.48e+1	7.10e+1	3.95e+1
90	1.40e+2	1.33e+2	8.61e+1	7.54e+1	7.18e+1	4.45e+1
100	1.40e+2	1.33e+2	9.53e+1	7.54e+1	7.18e+1	4.94e+1
	Cr			Fe		
E (MeV)	Electron	Positron	Photon	Electron	Positron	Photon
0.6	6.09e-2	5.78e-2	0	0	0	0
0.7	2.94e+0	2.36e+0	7.11e-5	2.02e+0	1.65e+0	4.69e-5
0.8	5.96e+0	4.41e+0	2.14e-4	5.17e+0	3.79e+0	2.16e-4
0.9	8.91e+0	6.28e+0	9.83e-4	8.38e+0	5.78e+0	6.56e-4
1.0	1.17e+1	8.02e+0	4.00e-3	1.15e+1	7.64e+0	2.92e-3
1.5	2.17e+1	1.47e+1	6.64e-2	2.29e+1	1.50e+1	6.47e-2
2.0	2.87e+1	2.00e+1	1.89e-1	3.08e+1	2.06e+1	1.96e-1
2.5	3.40e+1	2.42e+1	3.44e-1	3.67e+1	2.53e+1	3.67e-1
3.0	3.84e+1	2.79e+1	5.21e-1	4.16e+1	2.92e+1	5.65e-1
4.0	4.52e+1	3.39e+1	9.30e-1	4.92e+1	3.58e+1	1.02e+0
5.0	5.06e+1	3.87e+1	1.40e+0	5.52e+1	4.11e+1	1.56e+0
6.0	5.50e+1	4.27e+1	1.92e+0	6.00e+1	4.55e+1	2.15e+0
7.0	5.87e+1	4.62e+1	2.49e+0	6.41e+1	4.93e+1	2.81e+0
8.0	6.19e+1	4.92e+1	3.11e+0	6.76e+1	5.26e+1	3.53e+0
9.0	6.47e+1	5.19e+1	3.78e+0	7.07e+1	5.55e+1	4.30e+0
10	6.71e+1	5.43e+1	4.48e+0	7.35e+1	5.81e+1	5.12e+0
12	7.14e+1	5.85e+1	5.99e+0	7.82e+1	6.27e+1	6.87e+0
14	7.50e+1	6.20e+1	7.61e+0	8.21e+1	6.66e+1	8.77e+0
16	7.81e+1	6.51e+1	9.33e+0	8.55e+1	7.00e+1	1.08e+1
18	8.08e+1	6.77e+1	1.11e+1	8.85e+1	7.29e+1	1.29e+1
20	8.32e+1	7.01e+1	1.30e+1	9.11e+1	7.55e+1	1.51e+1
25	8.81e+1	7.52e+1	1.78e+1	9.66e+1	8.11e+1	2.07e+1
30	9.21e+1	7.92e+1	2.28e+1	1.01e+2	8.55e+1	2.66e+1
35	9.54e+1	8.26e+1	2.78e+1	1.05e+2	8.93e+1	3.26e+1
40	9.82e+1	8.55e+1	3.30e+1	1.08e+2	9.25e+1	3.87e+1
45	1.01e+2	8.80e+1	3.81e+1	1.10e+2	9.52e+1	4.48e+1
50	1.03e+2	9.02e+1	4.31e+1	1.13e+2	9.77e+1	5.08e+1
60	1.06e+2	9.39e+1	5.30e+1	1.17e+2	1.02e+2	6.26e+1
70	1.09e+2	9.70e+1	6.26e+1	1.20e+2	1.05e+2	7.40e+1
80	1.11e+2	9.95e+1	7.18e+1	1.22e+2	1.08e+2	8.50e+1
90	1.13e+2	1.02e+2	8.07e+1	1.25e+2	1.11e+2	9.56e+1
100	1.13e+2	1.02e+2	8.92e+1	1.25e+2	1.11e+2	1.06e+2
	Ni			Cu		
E (MeV)	Electron	Positron	Photon	Electron	Positron	Photon
0.6	0	0	0	1.65e+0	1.40e+0	3.97e-5
0.7	1.40e+0	1.16e+0	2.98e-5	6.96e+0	5.12e+0	4.66e-4
0.8	4.74e+0	3.44e+0	2.32e-4	1.23e+1	8.34e+0	1.17e-3

(*continued on next page*)

Table 3 (*continued*)

	Ni			Cu		
E (MeV)	Electron	Positron	Photon	Electron	Positron	Photon
0.9	8.25e+0	5.58e+0	6.09e-4	1.74e+1	1.12e+1	4.14e-3
1.0	1.17e+1	7.59e+0	2.49e-3	2.20e+1	1.39e+1	1.21e-2
1.5	2.48e+1	1.56e+1	6.70e-2	3.83e+1	2.41e+1	1.39e-1
2.0	3.37e+1	2.18e+1	2.13e-1	4.96e+1	3.22e+1	3.68e-1
2.5	4.04e+1	2.69e+1	4.06e-1	5.82e+1	3.88e+1	6.52e-1
3.0	4.59e+1	3.13e+1	6.32e-1	6.53e+1	4.45e+1	9.75e-1
4.0	5.45e+1	3.85e+1	1.16e+0	7.64e+1	5.40e+1	1.72e+0
5.0	6.11e+1	4.43e+1	1.78e+0	8.50e+1	6.16e+1	2.58e+0
6.0	6.65e+1	4.91e+1	2.48e+0	9.21e+1	6.80e+1	3.55e+0
7.0	7.10e+1	5.33e+1	3.26e+0	9.80e+1	7.35e+1	4.63e+0
8.0	7.49e+1	5.70e+1	4.11e+0	1.03e+2	7.83e+1	5.80e+0
9.0	7.84e+1	6.02e+1	5.02e+0	1.08e+2	8.25e+1	7.06e+0
10	8.14e+1	6.31e+1	6.00e+0	1.12e+2	8.64e+1	8.39e+0
12	8.67e+1	6.82e+1	8.09e+0	1.18e+2	9.31e+1	1.13e+1
14	9.11e+1	7.25e+1	1.04e+1	1.24e+2	9.87e+1	1.44e+1
16	9.48e+1	7.62e+1	1.28e+1	1.29e+2	1.04e+2	1.76e+1
18	9.81e+1	7.95e+1	1.53e+1	1.34e+2	1.08e+2	2.10e+1
20	1.01e+2	8.24e+1	1.79e+1	1.37e+2	1.12e+2	2.46e+1
25	1.07e+2	8.85e+1	2.47e+1	1.45e+2	1.20e+2	3.37e+1
30	1.12e+2	9.35e+1	3.17e+1	1.52e+2	1.26e+2	4.32e+1
35	1.16e+2	9.76e+1	3.88e+1	1.57e+2	1.32e+2	5.29e+1
40	1.19e+2	1.01e+2	4.61e+1	1.62e+2	1.37e+2	6.26e+1
45	1.22e+2	1.04e+2	5.32e+1	1.66e+2	1.41e+2	7.22e+1
50	1.25e+2	1.07e+2	6.03e+1	1.69e+2	1.44e+2	8.17e+1
60	1.29e+2	1.12e+2	7.42e+1	1.75e+2	1.50e+2	1.00e+2
70	1.33e+2	1.15e+2	8.76e+1	1.80e+2	1.55e+2	1.18e+2
80	1.36e+2	1.19e+2	1.00e+2	1.83e+2	1.60e+2	1.35e+2
90	1.38e+2	1.21e+2	1.13e+2	1.87e+2	1.63e+2	1.52e+2
100	1.38e+2	1.21e+2	1.25e+2	1.87e+2	1.63e+2	1.68e+2
	W			U		
E (MeV)	Electron	Positron	Photon	Electron	Positron	Photon
1.7	0	0	0	2.90e+0	4.63e-1	6.16e-4
1.8	0	0	0	1.38e+1	1.78e+0	8.93e-3
1.9	0	0	0	2.75e+1	3.34e+0	2.77e-2
2.0	0	0	0	4.26e+1	5.08e+0	5.70e-2
2.2	0	0	0	7.48e+1	8.90e+0	1.54e-1
2.4	8.31e-01	1.76e-01	9.09e-05	1.05e+2	1.29e+1	3.05e-1
2.5	2.45e+0	4.68e-1	5.37e-4	1.18e+2	1.50e+1	4.01e-1
3.0	1.51e+1	2.79e+0	1.41e-2	1.70e+2	2.48e+1	1.04e+0
4.0	3.97e+1	8.52e+0	1.60e-1	2.12e+2	4.16e+1	2.82e+0
5.0	5.29e+1	1.35e+1	4.71e-1	2.34e+2	5.58e+1	5.21e+0
6.0	6.14e+1	1.78e+1	9.38e-1	2.51e+2	6.81e+1	8.22e+0
7.0	6.81e+1	2.16e+1	1.56e+0	2.65e+2	7.89e+1	1.19e+1
8.0	7.36e+1	2.51e+1	2.34e+0	2.78e+2	8.85e+1	1.61e+1
9.0	7.83e+1	2.81e+1	3.25e+0	2.88e+2	9.71e+1	2.09e+1
10	8.23e+1	3.10e+1	4.30e+0	2.98e+2	1.05e+2	2.61e+1
12	8.92e+1	3.59e+1	6.72e+0	3.14e+2	1.19e+2	3.76e+1
14	9.48e+1	4.02e+1	9.51e+0	3.27e+2	1.31e+2	5.04e+1
16	9.95e+1	4.39e+1	1.26e+1	3.38e+2	1.41e+2	6.40e+1
18	1.04e+2	4.73e+1	1.60e+1	3.48e+2	1.51e+2	7.84e+1
20	1.07e+2	5.03e+1	1.95e+1	3.57e+2	1.59e+2	9.32e+1
25	1.14e+2	5.66e+1	2.90e+1	3.74e+2	1.76e+2	1.32e+2
30	1.20e+2	6.19e+1	3.90e+1	3.89e+2	1.91e+2	1.72e+2
35	1.25e+2	6.64e+1	4.93e+1	4.01e+2	2.04e+2	2.12e+2
40	1.29e+2	7.03e+1	5.97e+1	4.11e+2	2.14e+2	2.52e+2
45	1.32e+2	7.38e+1	7.01e+1	4.20e+2	2.24e+2	2.91e+2
50	1.35e+2	7.68e+1	8.04e+1	4.28e+2	2.32e+2	3.30e+2
60	1.40e+2	8.21e+1	1.01e+2	4.41e+2	2.47e+2	4.05e+2
70	1.45e+2	8.65e+1	1.20e+2	4.52e+2	2.59e+2	4.76e+2
80	1.48e+2	9.04e+1	1.39e+2	4.61e+2	2.70e+2	5.44e+2
90	1.51e+2	9.37e+1	1.57e+2	4.70e+2	2.79e+2	6.08e+2
100	1.52e+2	9.43e+1	1.74e+2	4.70e+2	2.80e+2	6.70e+2

References

[1] K. Nordlund, S.J. Zinkle, A.E. Sand, F. Granberg, R.S. Averback, R.E. Stoller, T. Suzudo, L. Malerba, F. Banhart, W.J. Weber, F. Willaime, S.L. Dudarev, D. Simeone, Primary radiation damage: A review of current understanding and models, J. Nucl. Mater. 512 (2018) 450–479, https://doi.org/10.1016/j.jnucmat.2018.10.027.

[2] R.E. MacFarlane, A.C. Kahler, Methods for Processing ENDF/B-VII with NJOY, Nucl. Data Sheets. 111 (2010) 2739–2890, https://doi.org/10.1016/j.nds.2010.11.001.

[3] S. Chen, Methods for calculating the (n,2n) reaction-induced damage cross section with different approaches of kinematics, Nucl. Instrum. Methods Phys. Res. Sect. B Beam Interact. Mater. At. 508 (2021) 41–48, https://doi.org/10.1016/j.nimb.2021.10.007.

[4] W. Yin, T. Zu, L. Cao, H. Wu, Development and verification of heat production and radiation damage energy production cross section module in the nuclear data processing code NECP-Atlas, Ann. Nucl. Energy. 144 (2020), 107544, https://doi.org/10.1016/j.anucene.2020.107544.

[5] Q. Zhao, H. Wu, X. Wu, P. Liu, Z. Ge, Development of KDC Program for Calculation of Factor of Neutron Kinetic Energy Released in Material and Radiation Damage Cross Section (in Chinese), At. Energy Sci. Technol. 51 (2017) 1557–1563.

[6] S. Chen, D. Bernard, Recommendation for computing neutron irradiation damage from evaluated nuclear data, J. Nucl. Mater. 562 (2022), 153610, https://doi.org/10.1016/j.jnucmat.2022.153610.

[7] S. Chen, Study of neutron capture reaction-induced displacement damage cross section and KERMA factor, Nucl. Instrum. Methods Phys. Res. Sect. B Beam Interact. Mater. At. 513 (2022) 1–8, https://doi.org/10.1016/j.nimb.2021.12.013.

[8] S.P. Simakov, U. Fischer, Displacement damage induced in iron by gammas and neutrons under irradiation in the IFMIF test cell, J. Nucl. Mater. 417 (2011) 1321–1324, https://doi.org/10.1016/j.jnucmat.2010.12.175.

[9] O.S. Oen, D.K. Holmes, Cross Sections for Atomic Displacements in Solids by Gamma Rays, J. Appl. Phys. 30 (1959) 1289–1295, https://doi.org/10.1063/1.1735307.

[10] N.P. Baumann, Gamma-ray Induced Displacements in D_2O Reactors, in: Proc. Seventh ASTM-EURATOM Symp. React. Dosim., Strasbourg, France, 1990: pp. 689–697.

[11] D.E. Alexander, Defect production considerations for gamma ray irradiation of reactor pressure vessel steels, J. Nucl. Mater. 240 (1997) 196–204, https://doi.org/10.1016/S0022-3115(96)00713-1.

[12] J. Kwon, A.T. Motta, Gamma displacement cross-sections in various materials, Ann. Nucl. Energy. 27 (2000) 1627–1642, https://doi.org/10.1016/S0306-4549(00)00024-4.

[13] K. Fukuya, I. Kimura, Calculation of Gamma Induced Displacement Cross-sections of Iron Considering Positron Contribution and Using Standard Damage Model, J. Nucl. Sci. Technol. 40 (2003) 423–428, https://doi.org/10.1080/18811248.2003.9715375.

[14] I. Piñera, C.M. Cruz, A. Leyva, Y. Abreu, A.E. Cabal, P.V. Espen, N.V. Remortel, Improved calculation of displacements per atom cross section in solids by gamma and electron irradiation, Nucl. Instrum. Methods Phys. Res. Sect. B Beam Interact. Mater. At. 339 (2014) 1–7, https://doi.org/10.1016/j.nimb.2014.08.020.

[15] S. Chen, D. Bernard, C. De Saint Jean, Calculation and analysis of gamma-induced irradiation damage cross section, Nucl. Instrum. Methods Phys. Res. Sect. B Beam Interact. Mater. At. 447 (2019) 8–21, https://doi.org/10.1016/j.nimb.2019.03.035.

[16] W.A. McKinley, H. Feshbach, The Coulomb Scattering of Relativistic Electrons by Nuclei, Phys. Rev. 74 (1948) 1759–1763, https://doi.org/10.1103/PhysRev.74.1759.

[17] M.J. Norgett, M.T. Robinson, I.M. Torrens, A proposed method of calculating displacement dose rates, Nucl. Eng. Des. 33 (1975) 50–54, https://doi.org/10.1016/0029-5493(75)90035-7.

[18] ISO 19226:2017, Nuclear energy — Determination of neutron fluence and displacement per atom (dpa) in reactor vessel and internals, 2017. https://www.iso.org/obp/ui/#iso:std:iso:19226:ed-1:v1:en (accessed June 24, 2020).

[19] J. Lindhard, V. Nielsen, M. Scharff, P.V. Thomsen, Integral equations governing radiation effects, Mat.-Fys. Meddelelser Konglige Dan, Vidensk. Selsk. 33 (1963) 1–42. http://gymarkiv.sdu.dk/MFM/kdvs/mfm%2030-39/mfm-33-10.pdf.

[20] M.T. Robinson, The Energy Dependence of Neutron Radiation Damage in Solids, in: Nucl. Fusion React., British Nuclear Energy Society, 1970: pp. 364–378. https://www.icevirtuallibrary.com/doi/abs/10.1680/nfr.44661.0025.

[21] S. Chen, D. Bernard, On the beta decay-induced radiation damage, Nucl. Instrum. Methods Phys. Res. Sect. B Beam Interact. Mater. At. 467 (2020) 58–64, https://doi.org/10.1016/j.nimb.2020.01.017.

[22] W.E. King, K.L. Merkle, M. Meshii, Threshold energy surface and frenkel pair resistivity for Cu, J. Nucl. Mater. 117 (1983) 12–25, https://doi.org/10.1016/0022-3115(83)90005-3.

[23] S.-L. Chen, Low-energy atomic displacement model of SRIM simulations, Nucl. Sci. Tech. 32 (2021) 119, https://doi.org/10.1007/s41365-021-00971-2.

[24] Y. Chen, K. Morishita, Molecular dynamics simulation of defect production in Fe due to irradiation, Nucl. Mater. Energy. 30 (2022), 101150, https://doi.org/10.1016/j.nme.2022.101150.

[25] J.C. Meyer, F. Eder, S. Kurasch, V. Skakalova, J. Kotakoski, H.J. Park, S. Roth, A. Chuvilin, S. Eyhusen, G. Benner, A.V. Krasheninnikov, U. Kaiser, Accurate Measurement of Electron Beam Induced Displacement Cross Sections for Single-Layer Graphene, Phys. Rev. Lett. 108 (2012), 196102, https://doi.org/10.1103/PhysRevLett.108.196102.

[26] J.C. Meyer, F. Eder, S. Kurasch, V. Skakalova, J. Kotakoski, H.J. Park, S. Roth, A. Chuvilin, S. Eyhusen, G. Benner, A.V. Krasheninnikov, U. Kaiser, Erratum: Accurate Measurement of Electron Beam Induced Displacement Cross Sections for Single-Layer Graphene [Phys. Rev. Lett. 108, 196102 (2012)], Phys. Rev. Lett. 110 (2013) 239902, https://doi.org/10.1103/PhysRevLett.110.239902.

[27] S. Chen, D. Bernard, L. Buiron, Study on the self-shielding and temperature influences on the neutron irradiation damage calculations in reactors, Nucl. Eng. Des. 346 (2019) 85–96, https://doi.org/10.1016/j.nucengdes.2019.03.006.

[28] Q. Yan, J. Wang, D. Chen, J. Gigax, L. Shao, Displacement cross sections of electron irradiated graphene and carbon nanotubes, Nucl. Instrum. Methods Phys. Res. Sect. B Beam Interact. Mater. At. 350 (2015) 20–25, https://doi.org/10.1016/j.nimb.2015.02.075.

[29] Astm, E521–96, Practice for Neutron Radiation Damage Simulation by Charged-Particle Irradiation, ASTM International, West Conshohocken, PA (1996), https://doi.org/10.1520/E0521-96.

[30] J.C. Bourgoin, P. Ludeau, B. Massarani, Threshold energy determination in thick semiconductor samples, Rev. Phys. Appliquée. 11 (1976) 279–284, https://doi.org/10.1051/rphysap:01976001102027900.

[31] E. Holmström, A. Kuronen, K. Nordlund, Threshold defect production in silicon determined by density functional theory molecular dynamics simulations, Phys. Rev. B. 78 (2008), https://doi.org/10.1103/PhysRevB.78.045202.

[32] A.Y. Konobeyev, U. Fischer, Y.A. Korovin, S.P. Simakov, Evaluation of effective threshold displacement energies and other data required for the calculation of advanced atomic displacement cross-sections, Nucl. Energy Technol. 3 (2017) 169–175, https://doi.org/10.1016/j.nucet.2017.08.007.

[33] S.J. Zinkle, C. Kinoshita, Defect production in ceramics, J. Nucl. Mater. 251 (1997) 200–217, https://doi.org/10.1016/S0022-3115(97)00224-9.

[34] S. Chen, D. Bernard, P. Tamagno, J. Tommasi, S. Bourganel, G. Noguère, C. De Saint Jean, Calculation and verification of neutron irradiation damage with differential cross sections, Nucl. Instrum. Methods Phys. Res. Sect. B Beam Interact. Mater. At. 456 (2019) 120–132, https://doi.org/10.1016/j.nimb.2019.07.011.

[35] N.F. Mott, The scattering of fast electrons by atomic nuclei, Proc. R. Soc. A. 124 (1929) 425–442, https://doi.org/10.1098/rspa.1929.0127.

[36] R. Idoeta, F. Legarda, Review and calculation of Mott scattering cross section by unscreened point nuclei, Nucl. Instrum. Methods Phys. Res. Sect. B Beam Interact. Mater. At. 71 (1992) 116–125, https://doi.org/10.1016/0168-583X(92)95312-F.

[37] M.J. Berger, M. Inokuti, H.H. Anderson, H. Bichsel, J.A. Dennis, D. Powers, S. M. Seltzer, J.E. Turner, ICRU Report 37: Stopping Powers for Electrons and Positrons, J. Int. Comm. Radiat. Units Meas. os19 (1984), https://doi.org/10.1093/jicru/os19.2.Report37.

[38] J.A. Bearden, A.F. Burr, Reevaluation of X-Ray Atomic Energy Levels, Rev. Mod. Phys. 39 (1967) 125–142, https://doi.org/10.1103/RevModPhys.39.125.

[39] H. Bethe, W. Heitler, On the stopping of fast particles and on the creation of positive electrons, Proc. R. Soc. A. 146 (1934) 83–112, https://doi.org/10.1098/rspa.1934.0140.

[40] C.M. Davisson, R.D. Evans, Gamma-Ray Absorption Coefficients, Rev. Mod. Phys. 24 (1952) 79–107, https://doi.org/10.1103/RevModPhys.24.79.

[41] H.A. Bethe, The influence of screening on the creation and stopping of electrons, Math. Proc. Camb. Philos. Soc. 30 (1934) 524–539, https://doi.org/10.1017/S0305004100012779.

[42] D.E. Cullen, Status Report, 2019.(accessed April 10, 2022, EPICS2017 (April 2019), https://www-nds.iaea.org/epics/DOCUMENTS/2019-EPICS2017-Status.pdf.

[43] E. Brun, F. Damian, C.M. Diop, E. Dumonteil, F.X. Hugot, C. Jouanne, Y.K. Lee, F. Malvagi, A. Mazzolo, O. Petit, J.C. Trama, T. Visonneau, A. Zoia, TRIPOLI-4®, CEA, EDF and AREVA reference Monte Carlo code, Ann. Nucl. Energy. 82 (2015) 151–160, https://doi.org/10.1016/j.anucene.2014.07.053.

[44] D.E. Cullen, J.H. Hubbell, L. Kissel, EPDL97: the Evaluated Photon Data Library, '97 Version, Lawrence Livermore National Laboratory, Livermore, US, 1997.

[45] O. Klein, Y. Nishina, Über die Streuung von Strahlung durch freie Elektronen nach der neuen relativistischen Quantendynamik von Dirac, Z. Für Phys. 52 (1929) 853–868, https://doi.org/10.1007/BF01366453.

[46] H. Hall, The Theory of Photoelectric Absorption for X-Rays and γ-Rays, Rev. Mod. Phys. 8 (1936) 358–397, https://doi.org/10.1103/RevModPhys.8.358.

[47] O.S. Oen, Cross sections for atomic displacements in solids by fast positrons, Nucl. Instrum. Methods Phys. Res. Sect. B Beam Interact. Mater. At. 33 (1988) 744–747, https://doi.org/10.1016/0168-583X(88)90672-6.

[48] K. Nordlund, S.J. Zinkle, A.E. Sand, F. Granberg, R.S. Averback, R. Stoller, T. Suzudo, L. Malerba, F. Banhart, W.J. Weber, F. Willaime, S.L. Dudarev, D. Simeone, Improving atomic displacement and replacement calculations with physically realistic damage models, Nat. Commun. 9 (2018) 1084, https://doi.org/10.1038/s41467-018-03415-5.

[49] S. Chen, Effective primary radiation damage model parameters for neutron irradiation experiments, J. Nucl. Mater. 568 (2022), 153883, https://doi.org/10.1016/j.jnucmat.2022.153883.